Purdue University
Purdue e-Pubs

Birck and NCN Publications | Birck Nanotechnology Center

1-2013

Nucleate boiling from smooth and rough surfaces - Part 1: Fabrication and characterization of an optically transparent heater-sensor substrate with controlled surface roughness

John P. McHale
Purdue University

Suresh V. Garimella
Birck Nanotechnology Center, Purdue University, sureshg@purdue.edu

Follow this and additional works at: http://docs.lib.purdue.edu/nanopub

 Part of the Nanoscience and Nanotechnology Commons

McHale, John P. and Garimella, Suresh V., "Nucleate boiling from smooth and rough surfaces - Part 1: Fabrication and characterization of an optically transparent heater-sensor substrate with controlled surface roughness" (2013). *Birck and NCN Publications.* Paper 1314.
http://dx.doi.org/10.1016/j.expthermflusci.2012.08.006

This document has been made available through Purdue e-Pubs, a service of the Purdue University Libraries. Please contact epubs@purdue.edu for additional information.

Experimental Thermal and Fluid Science 44 (2013) 456–467

Contents lists available at SciVerse ScienceDirect

Experimental Thermal and Fluid Science

journal homepage: www.elsevier.com/locate/etfs

Nucleate boiling from smooth and rough surfaces – Part 1: Fabrication and characterization of an optically transparent heater–sensor substrate with controlled surface roughness

John P. McHale, Suresh V. Garimella *

Cooling Technologies Research Center, an NSF IUCRC, School of Mechanical Engineering and Birck Nanotechnology Center, Purdue University, West Lafayette, IN 47907-2088, USA

ARTICLE INFO

Article history:
Received 21 February 2012
Received in revised form 30 July 2012
Accepted 9 August 2012
Available online 24 August 2012

Keywords:
Pool boiling
Nucleate boiling
Surface roughness
Heater design
ITO
Transparent conductive oxide

ABSTRACT

The effect of surface roughness on nucleate boiling heat transfer is not clearly understood. This study is devised to conduct detailed heat transfer and bubble measurements during boiling on a heater surface with controlled roughness. This first of two companion papers discusses details of the fabrication, construction, and operation of the experimental facility. Test pieces are fabricated from 50.8 mm × 50.8 mm × 3.18 mm borosilicate glass squares that are roughened by abrading with diamond compound with particles of known size and then annealed in order to control small-scale roughness features. Heater/sensor devices are fabricated by depositing indium tin oxide (ITO), a transparent electrically conductive material, on top of the roughened glass surfaces. A method for calibrating the ITO devices for use as temperature sensors is developed. Experimental boiling curves are reported for seven surfaces of different roughness tested in the perfluorinated fluorocarbon liquid, FC-72. The measured receding contact angle for FC-72 on the ITO-coated surfaces is reported. The wall superheat during saturated pool boiling at atmospheric pressure was found not to vary consistently with surface average roughness (R_a) values. Qualitative differences between smooth and rough surface boiling visualizations obtained simultaneously from the side and from below the heaters are discussed.

© 2012 Elsevier Inc. All rights reserved.

1. Introduction

Nucleate boiling is widely relied upon as a highly effective means of dissipating heat from critical devices such as nuclear fuel rods, power electronics, and propulsion devices. Often the device efficiency, performance and operational safety of the device are closely linked to the amount of power that can be dissipated while maintaining the temperature within specified system limits. The power dissipation bottleneck is linked to the resistance to heat flow into the coolant via nucleate boiling; it is desirable to reduce the wall superheat at all points of the boiling curve, and to predict it as closely as possible.

Surface condition was found to significantly affect the boiling curve even by early researchers such as Jakob [1]. Rohsenow [2] included a surface–fluid interaction factor C_{sf} in his widely used pool boiling correlation, acknowledging the role of surface structure and liquid contact angle. Subsequent researchers [3–6] showed that the presence of cavities of certain size and shape was a necessary condition for nucleation of bubbles. Several experiments (*e.g.*, [7–10]) have been conducted to ascertain values of wall superheat or C_{sf} for different surface roughness conditions. Surface roughness is a measurable quantity, and therefore a number of works [11–14] have tied their individual pool boiling heat transfer results to measured roughness parameters. The most commonly correlated roughness parameters are termed R values (R_a, R_q, R_p, etc.). Several correlations covering a wide range of fluids and R values are available, and were recently reviewed by Jones et al. [15]. Inconsistencies between experimental results and predictions from R-based correlations have been noted by several authors [14–17]. Jones [18] proposed a modification of the roughness factor in the Cooper [19] correlation, which somewhat decreased errors in predicted h values vs a large number of data sets from the literature.

It is widely acknowledged in the literature that the boiling curve must depend on details of the nucleating bubbles, namely the nucleation site density, bubble departure size and growth rate, and frequency of ebullition. The nucleation site density correlation of Hibiki and Ishii [20] is fairly definitive and agrees with the extant data to within approximately 50% – an impressive statistic considering the many orders of magnitude spanned. No broad, uniformly applicable correlation is available for bubble departure diameters and frequencies, however, though a couple of recent models [21,22] have reported progress. A survey of the literature on the subject (see, *e.g.*, Carey [23]) reveals that there is a lack of agreement even on the important independent variables that should be considered. McHale and Garimella [24] recently showed

* Corresponding author. Tel.: +1 765 494 5621.
E-mail address: sureshg@purdue.edu (S.V. Garimella).

0894-1777/$ - see front matter © 2012 Elsevier Inc. All rights reserved.
http://dx.doi.org/10.1016/j.expthermflusci.2012.08.006

Nomenclature

C	convection constant
C_{sf}	Rohsenow [2] surface–fluid interaction factor
d_p	particle diameter (m)
h	heat transfer coefficient (W/m^2 K)
i	counting index in summations
k	thermal conductivity (W/m K)
n	maximum value of counting index in summations
R	electrical resistance (Ω)
R_p	vertical roughness parameter (μm)
R_a	average roughness (μm)
R_q	root-mean-square roughness (μm)
q	heat flux (W/cm^2)
t	time (s)
T	temperature (K) (unless °C is specified)
ΔT	temperature difference with respect to saturation (K) or (°C)
x	lateral surface length dimension (m)
y	lateral surface width dimension (m)
z	vertical surface height dimension (m)

Greek

θ	liquid side contact angle (°)
ω	under relaxation factor in Eqs. (5)–(7), dimensionless

Subscripts

app	apparent
anneal	annealing
calc	calculated value
exp	experimental value
high	highest of data set
low	lowest of data set
loss	heat flux loss from test strip by spreading through substrate
max	maximum
nc	of natural convection
new	next iteration value, Eqs. (5)–(7)
nom	nominal
old	current iteration value, Eqs. (5)–(7)
p	particle
r	receding
s	of the solid
sat	at saturation
tot	total heat flux
w	of the heated wall
∞	convection ambient

Superscripts

*	value normalized by value at saturation

that surface roughness had an effect on departure diameter and frequency in pool boiling of the dielectric liquid, FC-77.

The present work aims to improve the understanding of the effect of surface roughness on nucleate boiling heat transfer. A new experimental facility is devised in which the heater surface and its roughness are well characterized, pool boiling is exhaustively visualized for each test condition, and automated bubble measurements are obtained from the visualizations. Details of the fabrication, design, and operation of the experimental facility and test pieces are reported here. Characterization of test surface roughness is discussed, and then the boiling heat transfer results are presented. In a companion paper [25], a characteristic length scale is developed for boiling from rough surfaces and new surface roughness measures are defined. The automated measurement technique employed for bubble measurements is assessed. Analysis of the heat transfer and bubble measurements is finally performed, elucidating trends that may contribute to the development of comprehensive correlations based on surface roughness.

2. Device fabrication

Seven optically transparent heater–sensor test pieces with different scales of surface roughness were prepared for this work. The transparent substrates allowed for simultaneous visualizations of boiling to be obtained from the side and from below the heater. Fabrication of the boiling substrates required three steps as described below: (1) surface roughening, (2) heater material coating, and (3) patterning.

2.1. Surface roughening

Blanks of 50.8 mm × 50.8 mm × 3.18 mm borosilicate float glass squares (McMaster-Carr 8476K121) with both sides initially smooth served as the starting material. Surface roughness was imparted to one side of each part by abrading with a diamond paste (Kay Diamond Products KG3013) containing particles of a known size range. The details of the surface preparation process were as follows.

First, the test piece blanks were fixed into a wood block containing a shallow recess with double-sided tape. A small amount of diamond paste and several drops of lubricating oil (Edge liquid) were placed on the abrasion surface, a 153 mm × 153 mm sheet of borosilicate float glass. The abrasive slurry was mixed and spread with a fingertip, and then the wood block fixture containing the test blank was pressed against the abrasive. The fixture was moved repeatedly in a random, somewhat circular path with 100 repetitions. The roughened test blanks were then removed from the block and cleaned thoroughly in order in soap and water, toluene, acetone, and then isopropyl alcohol. Cleaning with the latter three solvents was conducted for 5 min each in an ultrasonic cleaner.

Following roughening and cleaning, the blanks were annealed in a tube furnace (Blue M model STF55321C) at temperatures of at least 725 °C to remove radial and lateral cracks below the surface (see, *e.g.*, [26]) which may otherwise act as invisible vapor trap sites. Different annealing conditions were applied to some surfaces in order to vary not only the size of roughness features, but their structure as well. Abrasive particle nominal diameters $d_{p,nom}$, annealing conditions, and resulting surface average and rms roughnesses (R_a and R_q, respectively) of each test substrate are listed in Table 1. SEM images of 250-μm particle abraded surfaces annealed under different conditions are shown in Fig. 1 to show the effect of annealing conditions on surface structure.

2.2. Heater material coating

After annealing, the roughened faces of the parts were conformally coated with approximately 250 nm of indium tin oxide (ITO) using a sputtering technique. The resulting coated surfaces exhibited either a yellow or blue–indigo color, depending upon the coating batch. Following ITO coating, the parts were again cleaned in toluene, acetone, and then methanol. 10 nm of titanium as an adhesion layer and then 200 nm of gold were evaporated

Table 1
Test substrate parameters.

Device no.	$d_{p,nom}$ (μm)	T_{anneal} (°C)	t_{anneal} (min)	$R_{a,low}$ (μm)	$R_{a,high}$ (μm)	$R_{q,low}$ (μm)	$R_{q,high}$ (μm)
1	–	–	–	0.263	0.341	0.319	0.423
2	15	725	5	0.622	0.726	0.789	0.930
3	30	740	15	1.396	1.649	1.755	2.09
4	100	725	5	4.25	5.17	5.22	6.66
5	250	725	5	7.51	13.04	9.13	16.46
6	100	740	15	4.40	5.48	5.41	7.16
7	100	750	45	3.73	5.04	4.58	6.38

successively onto the ITO surface to provide for isopotential electrical contacts.

2.3. Patterning

The parts were then subjected to a 2-step conventional microlithography process in order to pattern ITO heater strips and gold contacts. The photolithography mask patterns are shown in Fig. 2. Before each of the two steps, the test pieces were cleaned in toluene, acetone, and isopropanol for 5 min each, then prebaked for 10 min in a 90 °C oven to drive off residual liquid molecules. AZ-9260 (AZ Electronic Materials USA Corp.) positive photoresist (PR) was applied to the surface by spinning at 4000 rpm for 40 s, with a 2-s ramp up in order to prevent the relatively massive test piece from slipping off the spinner vacuum chuck. The resulting PR thickness for the spin recipe was approximately 7 μm [27], enough to coat even the largest asperities (as verified by visual inspection under a microscope). The PR-coated parts were softbaked in a 110 °C oven for 4 min, then inserted into the mask aligner (Karl Suss model MJB-3). After aligning the mask to the part, the coated surface was subjected to UV light from the aligner's internal mercury arc lamp at an intensity of 1200 mJ/cm^2 for 36 s. Following exposure, the test pieces were developed in a 3:1 solution of water and AZ 400 K for 2 min, and then hardbaked in a 90 °C oven for 10 min.

In the first patterning step, the entire heater and marker array was patterned by successively etching the gold, titanium, and ITO layers, removing all areas not appearing black in Fig. 2a. In the second patterning step, the photoresist was patterned according to the black areas of Fig. 2b. Only gold and titanium were removed in this step, leaving the ITO pattern unmodified.

The 200-nm gold layer was removed in approximately 2 min by immersion in a gold-specific etchant containing potassium iodate (Transene Gold Etch TFA). The 10-nm titanium adhesion layer was then etched using "base piranha" solution consisting of three parts $NH_4(OH)$ (29% by mass in water) to 1 part H_2O_2 (30% by mass in water), requiring about 30 s for complete removal. The ITO layer was etched in concentrated HCl (37% by mass in water), a process that required soaking between 5 and 15 min depending upon the ITO coating batch. Undercutting of up to 10 μm was observed, the HCl etch being anisotropic and local etch rates being highly dependent upon the material composition and/or surface geometry. After etching, the photoresist etch stop was removed by soaking in toluene, followed by acetone and then isopropanol.

Completed parts (see Fig. 3) contained four test strips of different widths flanked by gold electrodes with good adhesion and electrical contact properties, with minimum separations of 1 mm between electrical contacts for different strips. The test strips chosen for this study measured 25 mm long × 400 μm wide, a width which was found experimentally to provide an optimum combination of heat transfer data and bubble visualization. Each completed part also contained a 25 mm long × 16 mm wide test area so that sessile drop contact angle measurements could be performed on a large ITO-coated area.

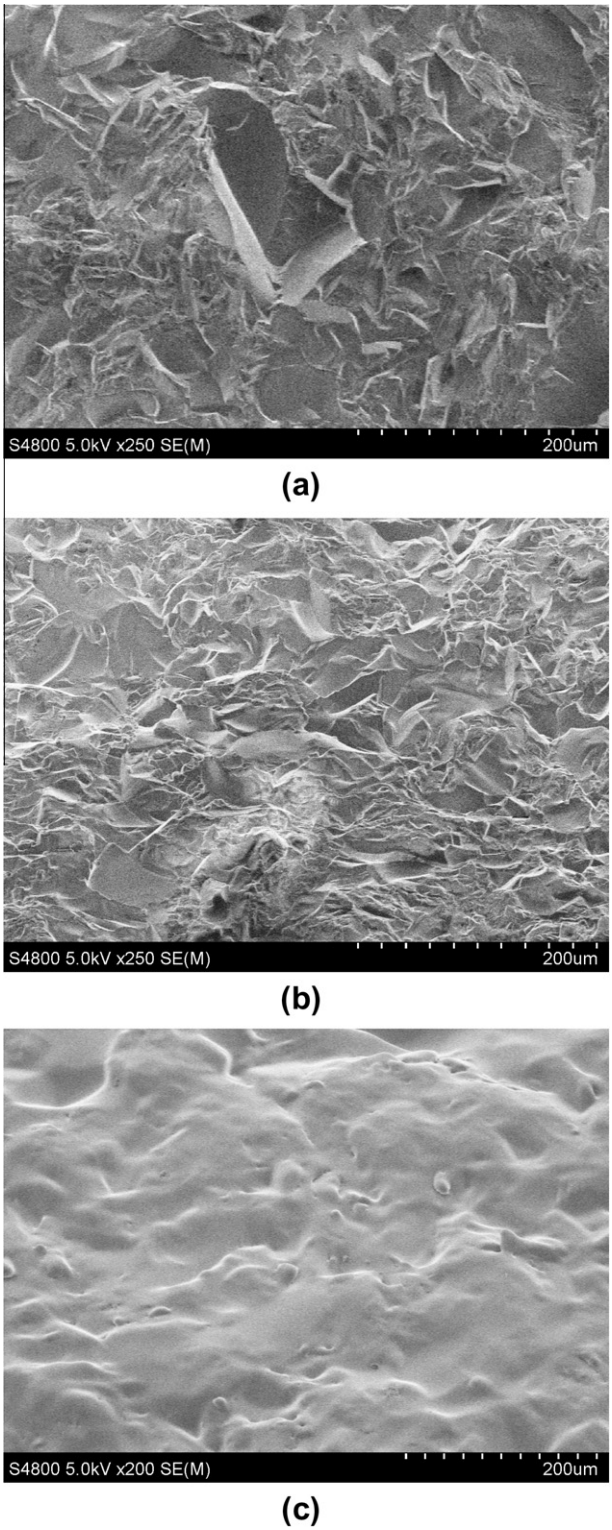

Fig. 1. SEM photos of surface morphology change of roughened borosilicate glass with increasing annealing temperature and soak time: (a) 725 °C × 5 min, (b) 740 °C × 15 min, and (c) 750 °C × 45 min.

3. Experimental facility

The experimental facility (shown in Fig. 4) for the boiling tests was designed to be operated as a sealed system with good thermal control and good optical and electrical access for a wide variety of measurements. The potential for chemical incompatibility across many possible working fluids also required the number of

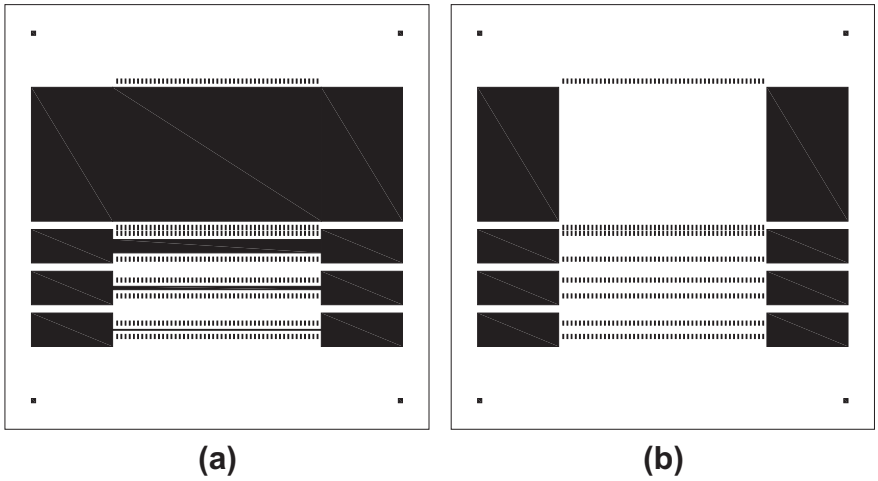

Fig. 2. Two-stage mask used in pattern definition of (a) ITO, and (b) metallization.

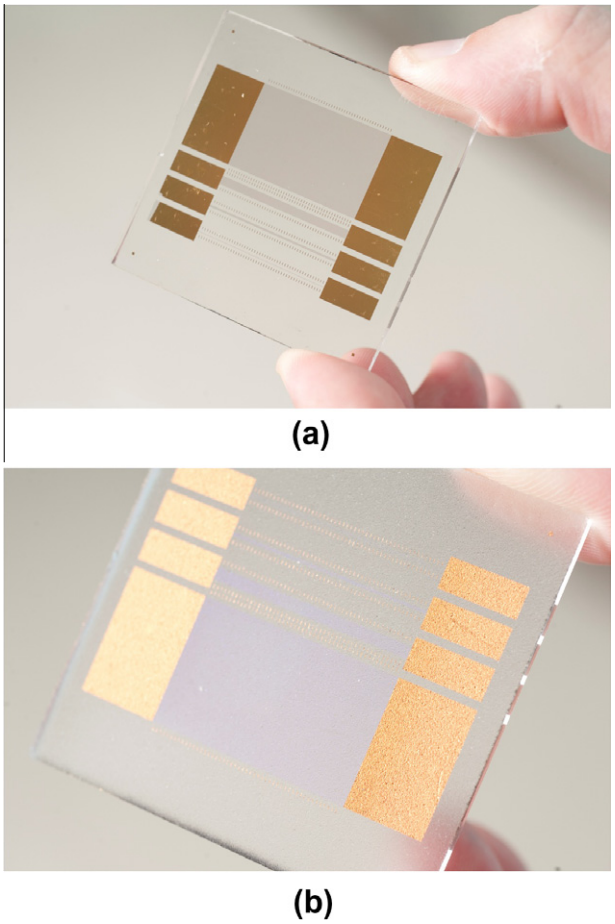

Fig. 3. Photos of completed boiling test pieces: (a) surface 1, polished – reverse side, and (b) surface 4, 100-μm particle abraded – top side.

materials used in the facility to be limited. Plastics were avoided whenever possible.

The working fluid used in the present tests, FC-72, has a low thermal conductivity relative to water – approximately 0.06 W/m K at 25 °C [28]. In addition, the refractive index of FC-72 changes moderately with temperature [29], which could result in severe index gradients and thus significant local image distortions if the liquid pool temperature were allowed to stratify. Optical access was required from four directions, complicating the application of a uniform temperature boundary condition preventing thermal stratification in the pool. The conflicting optical and thermal requirements were resolved as follows.

3.1. Sealing

The chamber was constructed of six PEEK sheets, each 19 mm thick (except for the 23.8-mm thick floor), fastened together to form an airtight thermally insulating box. PEEK was chosen as the wall material due to its excellent mechanical properties and chemical inertness, along with its robustness through thermal cycling. The four walls were bonded using an epoxy sealant (Loctite Hysol E-214HP) known to have good compatibility with fluorochemical liquids, and were held together with screws at each joint. PTFE gaskets separated the floor and ceiling of the chamber from the walls; screws from floor and ceiling into the walls maintained seals at the joints when assembled. Rectangular borosilicate glass viewing windows measuring 76.2 mm wide × 50.8 mm high × 4.76 mm thick were located in the front and rear walls of the chamber, as well as in the ceiling. These were sealed with PTFE-encapsulated rubber o-rings. The transparent test piece was set into a raised platform in the center of the chamber floor, also sealed from below with a similar o-ring. Each glass sealing part (including the test piece) was held in place by one or two PEEK clamping parts screwed into the facility box.

3.2. Thermal control

The walls, floor, and ceiling of the chamber contained drilled channels through which a secondary heating/cooling fluid was passed in order to fix the temperature of the pool. Also in the secondary fluid loop, a coiled stainless steel tube mounted in the ceiling of the chamber acted as a condenser to the working fluid when necessary. An immersion-style cartridge heater was installed at the lowest point of the pool in order to bring the working fluid rapidly up to the saturation temperature and to allow the chamber to be degassed by vigorous boiling. Heat was rejected from the cooling loop by a fan-cooled multipass finned heat exchanger. A second pane of glass separated by a 25-mm sealed air gap was used to create an adiabatic boundary below the test piece. The bottom pane was coated with ITO for resistive heating and maintained within 5 °C of the saturation temperature. Finally, hot air close to the saturation temperature was directed at the front glass viewing win-

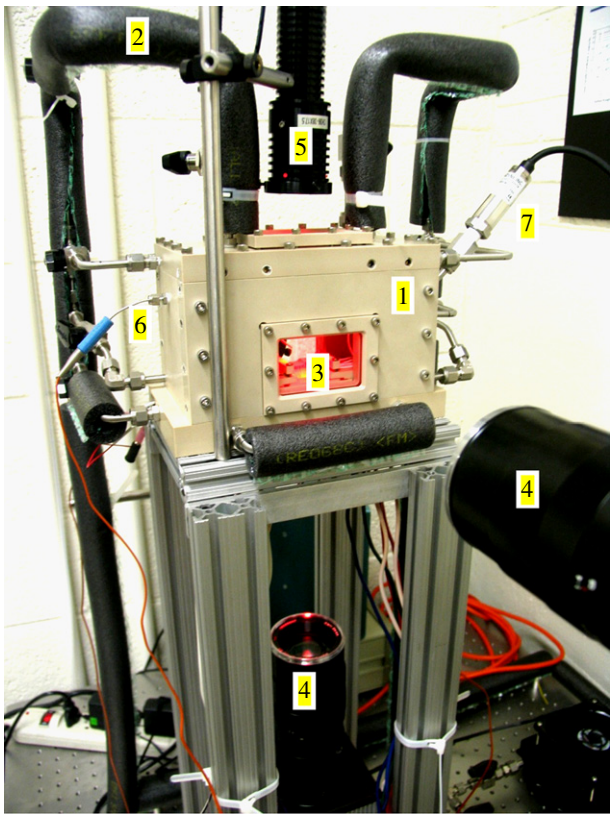

Fig. 4. Photo of experimental facility showing: (1) pool chamber, (2) secondary thermal loop, (3) test piece, (4) high speed cameras, (5) synchronized LED backlight, (6) pool thermocouple, and (7) pool pressure transducer.

dow in order to prevent excess heat transfer at this surface (which would otherwise lead to changes in refractive index of the working fluid and significant optical measurement errors).

3.3. Instrumentation and optical access

In order to provide power and measurement across the four test strips on the test piece, 16 sealed electrical couplings, eight on each side, were fixed into the floor of the pool chamber and sealed with E-214HP epoxy. Each heater/sensor was connected to the couplings in a 4-wire arrangement, with one pair of PTFE-coated lead wires and couplings carrying current and the other pair measuring the voltage drop across the electrodes. Two gold-coated spring-loaded pins with hemispherical tips made contact with each electrode. The electrical contact resistance of each spring contact was measured to be approximately 0.1 Ω; all other connections in the power and instrumentation loops had resistances that were negligible in comparison. Solder joints between PTFE-coated lead wires within the pool and the spring pins were coated with E-214HP epoxy to prevent migration of metallic species from/to the solder joint. Because the working fluid FC-72 has a very high electrical resistivity (1.0×10^{15} Ω cm), it was unnecessary to electrically passivate either the test strips or the electrical connections exposed to the fluid.

Complete optical access to the test strips with backlighting illumination was desired from two orthogonal directions. The maximum field of view for wide-angle recording (as in the present work) was just over 25 mm and the working distance was approximately 20 cm through combined media, primarily air. Minimum window dimensions of 50.8 mm were chosen to accomplish wide angle viewing and allow sealing using clamping retainer components.

3.4. Imaging and instrumentation

Two high-speed cameras were used to record boiling images of the entire heater strip at 4000 frames per second, with 1/12,000 s exposure time. For the side view, a Photron Ultima APX was used at 1024×512 resolution, while for the bottom view, a Photron 1024-PCI at 1024×256. Both cameras were equipped with identical macro-lenses (Carl Zeiss Makro-Planar T^* 2/100, optical power 2×) set at a focal length of 100 mm and aperture f/2.8. The spatial resolution was 34.3 μm/pixel ±0.1%.

Backlighting for the bottom and side view images was provided by two red LED light sources (Lightspeed Technologies model HPLS-36) pulsing alternately. The LEDs were synchronized with the two high-speed cameras utilizing a TTL-level pulse/delay generator (Berkeley Nucleonics model 555). The pulse width for illumination (proportional to image intensity), generally about 3 μs, was varied within ±2 μs for best image quality depending upon the surface and boiling characteristics at each test point.

The pool temperature was monitored with a type-T thermocouple attached to the terminals nearest the internal reference junction of an Agilent 34970A data acquisition system and was accurate to within 0.5 °C. The pool pressure was measured with a digital pressure transducer (Omegadyne PX409-030A) and maintained at 102,700 ± 1400 Pa. Heating and cooling for the secondary fluid loop was provided by a ThermoFisher Scientific Neslab EX17 circulating heater/chiller. The thermal control fluid was a 50/50 mix of water and ethylene glycol and was maintained between 61 and 67 °C in order to maintain the pool at the desired pressure and temperature, compensating for heat losses from the facility.

The electrical power to the test strip was provided by a Kepco JQE DC power supply capable of output between 0–150 V and 0–1.5 A. All electrical measurements were made using the Agilent data acquisition system. Voltage was measured directly, while current measurements were taken as voltage readings across precision shunt resistors (accuracy ± 0.1%) placed in series with a test strip. The uncertainty of the Agilent voltage measurements was negligible compared to uncertainties in temperature and heat flux discussed later in this work. High-accuracy 4-wire resistance measurements were made by the Agilent system for each unpowered test strip and shunt resistor (in unpowered state) between each test point to avoid significant uncertainties due to resistor accuracy. Banana plug test leads were used to switch quickly between powered and unpowered measurement states for the heater strip.

4. Experimental method

Power-controlled boiling curves with decreasing heat input are reported in this work, including 13–14 data points collected for each test surface. Boiling tests were conducted after first degassing the facility by vigorous boiling from the pool heater for 30 min combined with periodic venting. Once the temperature and pressure in the system stabilized at the expected saturation temperature (57 °C) and pressure (102,700 Pa) for a period of several minutes, the degassing procedure was deemed complete.

Large boiling incipience temperature overshoots are common for the Fluorinert liquids (see, *e.g., Jones* et al. [15]). To circumvent these temperature overshoots, the voltage input for each data point was initiated at a high enough value to initiate vigorous transition boiling (at a nominal heat flux of approximately 200 kW/m^2) and allowed to stabilize for a few seconds before decreasing or increasing input voltage to the desired value. Voltage set points were chosen based on the apparent value of critical heat flux and the onset of nucleate boiling (ONB). The actual power dissipation and temperature were calculated later from the heater/sensor test strip electrical data.

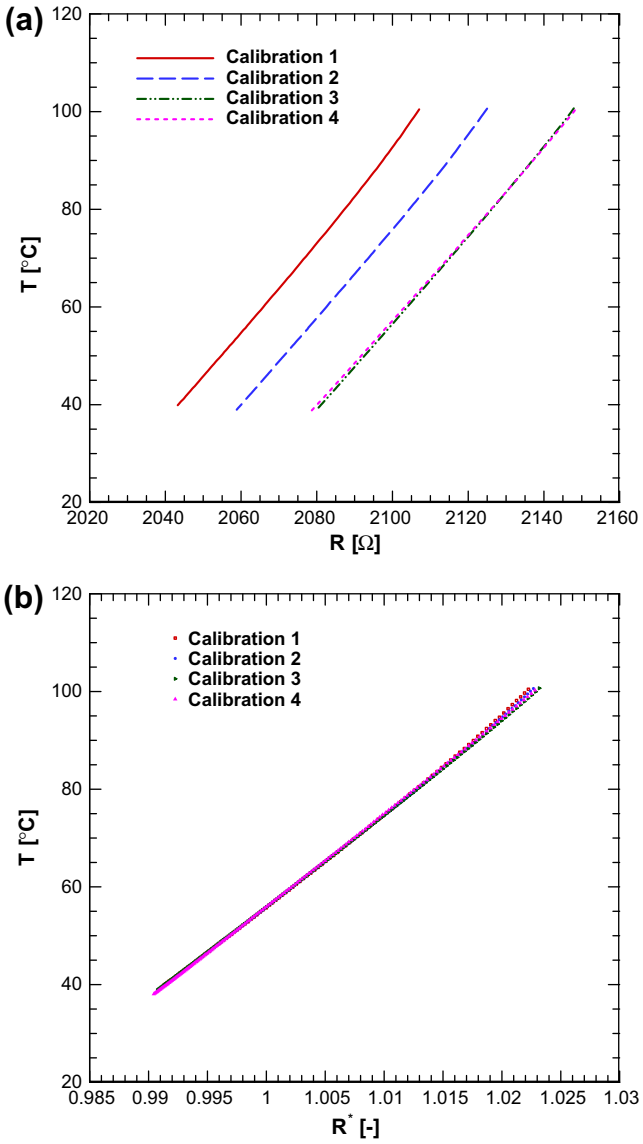

Fig. 5. Repeatability of the temperature vs resistance calibration curves for the 400-μm test strip of surface 5: (a) unrepeatable results for unmodified resistance values, and (b) repeatable results using resistance values normalized according to Eq. (1).

4.1. Temperature sensor calibration

ITO exhibits an approximately linear change in resistance with changes in temperature [30]. The patterned traces on the substrates in this work were intended to function as both heaters and as resistance temperature devices (RTDs) after calibration. The resistance of each single ITO device, however, was found to be extremely sensitive to atmospheric exposure, electrical activity, exposure to elevated temperature, and other long-term aging effects. This sensitivity of ITO device resistivity, which was noted by Pascual et al. [30] and Gregory and You [31], is likely due to small changes in chemical composition and the fact that conduction of electrons within the ternary compound may occur by several methods [32].

A fast calibration approach was adopted in order to circumvent long-term aging effects. Prior to testing each surface, the entire base of the facility, including the installed test piece, was placed in an oven exposed to an ambient atmosphere. A small thermocouple was affixed to the boiling surface with Kapton tape, which was then covered with a 12-mm thick layer of closed-cell silicone foam insulation. The oven temperature was set to the upper limit of the calibration, 100–120 °C, the maximum temperature allowable before damaging the test leads. Once the measured temperature stabilized, power to the oven was turned off. The resistance of all four test strips and the affixed thermocouple were simultaneously recorded as the interior of the oven cooled down over a period of approximately 2 h to 10 °C below the saturation point. It is noted that the thermal time constant of the test piece including the air gap was observed to be significantly less than that of the oven system.

Sample calibration curves over repeated tests are shown in Fig. 5a for the 400-μm test strip of surface 5. Multiple tests, however, revealed large-scale shifts in the calibration curve. The resistance values $R(T)$ of each test strip at a temperature T were therefore normalized by their "baseline" resistance $R(T_{sat})$ at temperature T_{sat}:

$$R^*(T) \equiv \frac{R(T)}{R(T_{sat})}. \quad (1)$$

T vs R^* curves were highly repeatable, as shown in Fig. 5b. A 2nd-degree polynomial (with little deviation from a straight line, except at high temperatures) was fit to the tabulated T vs R^* values; all temperatures reported in this work are those calculated from the individual curve fits for each test strip. The baseline resistance $R(T_{sat})$ was measured for each data point during boiling tests, since the resistance of the strip was often observed to change by unexpected amounts, indicating an in situ shift of the T vs R curve either to the right or left.

During boiling tests, both the applied voltage and the current through the heater were measured for a sufficient period of time for the voltage and current to reach a steady state (at least 5 min). Both the input power to the strip and its resistance were determined from the measured voltage and current. Immediately prior to recording steady-state data, synchronized high-speed videos were taken for 0.5 s. Bubble ebullition behavior was extremely consistent over time for each test condition, and 0.5 s was long enough to capture many consecutive ebullition cycles.

Between individual tests for successive data points, power to the test strip was shut off and the system temperature was allowed

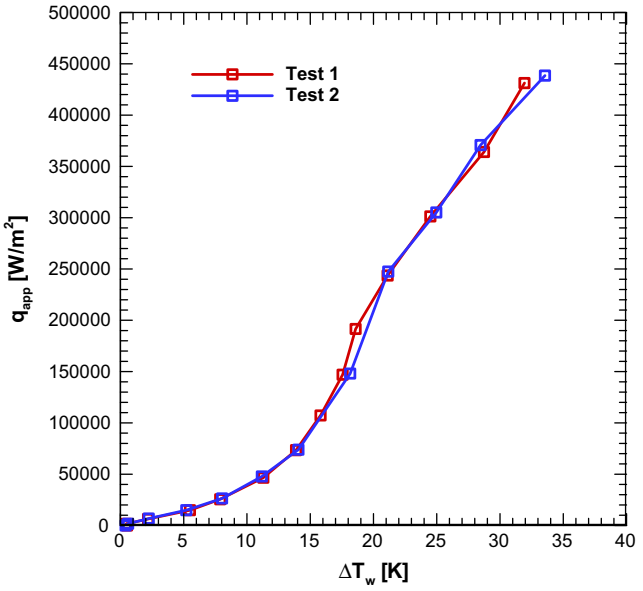

Fig. 6. Apparent boiling curves (heat flux uncorrected) measured by the 400 μm × 25 mm ITO heater/sensor test strip of surface 5. Good repeatability was obtained between tests.

Table 2
Receding contact angles of FC-72 on ITO were measured for all surfaces by: (a) imaging with a backlit goniometer, (b) absolute differencing of the image with a clean reference frame, and (c) fitting a spherical cap to the upper surface of the thresholded droplet image.

	(a)	(b)	(c)	
Surface 1 polished no anneal	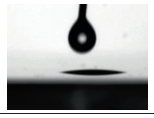		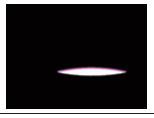	$\theta_r = 11.4°$ $\pm 0.4°$
Surface 2 $d_p = 15$ μm 998 K × 5 min. anneal	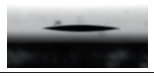	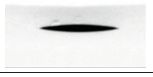		$\theta_r = 10.9°$ $\pm 0.7°$
Surface 3 $d_p = 30$ μm 1013 K × 15 min.	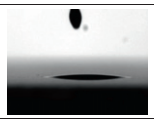	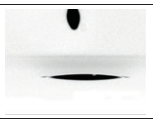	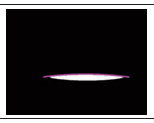	$\theta_r = 9.5°$ $\pm 0.4°$
Surface 4 $d_p = 100$ μm 998 K × 5 min.		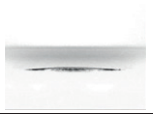	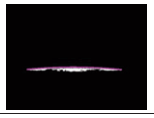	$\theta_r = 5.6°$ $\pm 0.6°$
Surface 5 $d_p = 250$ μm 998 K × 5 min.	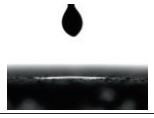		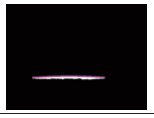	$\theta_r = 4.7°$ $\pm 1.0°$
Surface 6 $d_p = 100$ μm 1013 K × 15 min.			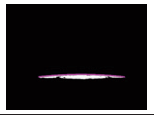	$\theta_r = 5.4°$ $\pm 0.5°$
Surface 7 $d_p = 100$ μm 1023 K × 45 min.		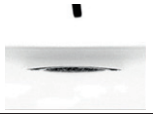	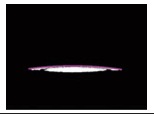	$\theta_r = 6.3°$ $\pm 0.7°$

to equilibrate for a period of 5 min, during which the heater surface temperature returned to the saturation point. During this time, the four test leads to the test strip were switched between terminal connections on a junction box so that the resistance of the unpowered strip at temperature T_{sat} could be measured by the data acquisition system.

4.2. Repeatability

Good repeatability of data obtained with this procedure was confirmed by repeating the test for surface 5, as shown by the results (apparent heat flux, uncorrected for thermal spreading in the substrate vs wall superheat) plotted in Fig. 6. The mean absolute discrepancy (*MAD*) between the two boiling curves accounting for differences in heat flux, defined as:

$$MAD = \frac{1}{n}\sum_{i=1}^{n} \mathrm{abs}\left[\frac{(\Delta T_{1,i} - \Delta T_{2,i})}{\Delta T_{1,\max}}\frac{(q_{1,i} - q_{2,i})}{q_{1,\max}} \cdot \left(\frac{d(\Delta T)}{dq}\right)_{1,i}\right], \qquad (2)$$

which accounts for differences in both heat flux and temperature, was 1.1% (percent of full scale). The mean discrepancy [*MD*, same definition as Eq. (2), but the term in brackets may carry a negative sign] was only 0.2% full scale, indicating that the boiling curves as a whole were not significantly different. When normalizing the discrepancy between each pair of points by their average magnitude rather than the full-scale value, *MAD* was 2.5% and *MD* was 0.7%. The practical temperature uncertainty of the facility, incorporating all factors, is therefore taken to be 2.5% for a single point and 1.1% for an entire curve below the maximum calibration temperature (100–120 °C). Above this temperature, linear extrapolations of the calibration curves were used.

4.3. Contact angle measurements

The liquid contact angle θ is an important parameter in modeling boiling characteristics such as nucleation site density [20] and bubble departure diameter [23,33]. Static contact angle may be the most important parameter representing the interaction between the fluid and specific nucleation sites [20,34,35], although dynamic wetting phenomena may also be important [36,37]. Dynamic contact angles are known to be a strong function of interface velocity [38] and can affect the size and growth rate of vapor bubbles under certain conditions [39]. Robust investigation of these effects is beyond the scope of the current work, but it is clear from the literature that θ must be considered in some form whenever surface effects are evaluated.

The receding contact angle θ_r was measured for sessile, evaporating FC-72 droplets of 5 μl initial volume on surfaces 1–7, as given in Table 2. Measurements were conducted on an unheated substrate at room temperature (23 °C) open to the laboratory environment. The evaporating receding angle was nearly independent of droplet size (an observation consistent with detailed evaporating droplet studies [40,41]). Static contact angles appeared to be less than 50% higher than the receding angles, but could not be precisely measured due to evaporation. Receding angles, however, could be measured repeatably, with small uncertainties.

Optical effects due to the roughness of several of the surfaces prevented the goniometer (Rame-Hart Model 290) from distinguishing the droplets for all surfaces, especially when color inversion occurred for very rough surfaces and low-angle droplets. The images from the goniometer – Table 2a – were therefore differenced with a clean (droplet-free) reference image – Table 2b, thresholded and finally fit with a circular arc – Table 2c – in order to

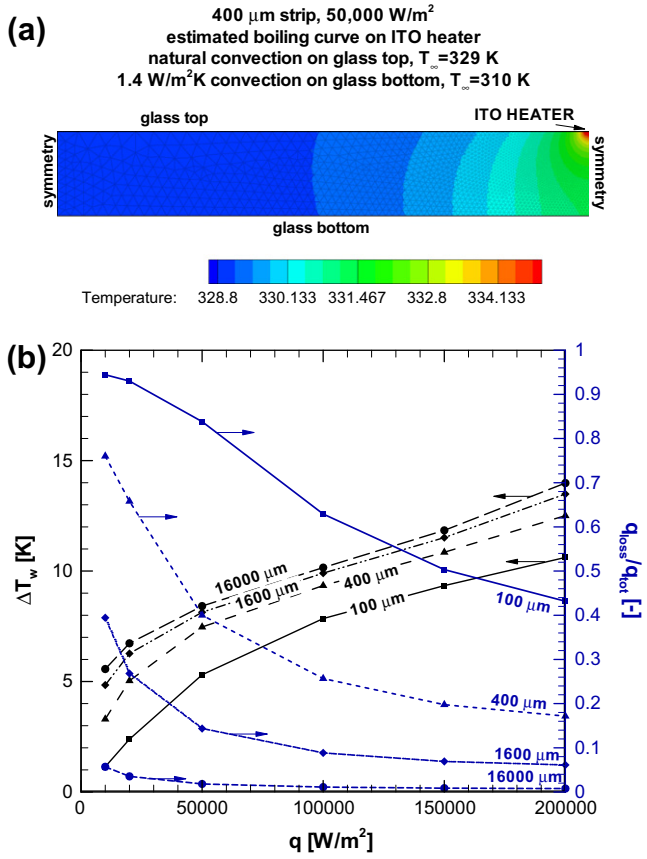

Fig. 7. Results of heat spreading simulations under simplified assumptions: (a) temperature contours for the 400-μm heater strip at q_{app} = 50,000 W/m^2; and (b) estimated effects of heater size and heat flux on the ratio of heat loss by spreading to total heat input.

Table 3
Overall error in wall superheat of apparent boiling curves (heat loss simulation vs experimental values).

Device no.	$R_{a,low}$ (μm)	RMS error (K)
1	0.263	0.843
2	0.622	0.568
3	1.396	0.746
4	4.25	0.375
5	7.51	0.332
6	4.40	0.531
7	3.73	0.470

determine the contact angle. In the differencing operation, intensity values between 0 and 1 of each pixel in the reference image were subtracted from the corresponding values in the droplet image and the absolute value of the result was increased in contrast by 200%. Forty or more samples were analyzed for each surface (except for surface 5, for which 22 samples were analyzed), resulting in uncertainties between 0.4° and 1.0°. The contact angles decreased almost monotonically with measured R_a values.

5. Data reduction

5.1. Heat loss calculation

In constructing boiling curves, the temperature data (abscissa) could be easily calculated from the calibration curves described in Section 4.1. The boiling heat flux data (ordinate), however, could not be obtained in a similar direct manner. The power dissipation, or apparent heat flux q_{app}, and the heater area were known to high accuracy, but a significant amount of heat was dissipated into the fluid after conduction through the substrate to areas beyond the heater strip. The adiabatic boundary condition provided by the heated double pane arrangement below the test surface minimized heat loss from the test strip, but the spreading effect was still significant.

A 2-D numerical model was implemented in the commercial software program, FLUENT [42], in order to estimate the heat loss and boiling heat flux for test strips of different width under the following assumptions. The model consisted of a 3.18 mm × 20 mm rectangular solid domain representing a cross section of the glass test piece as shown in Fig. 7a. Symmetry conditions were imposed on the right and left boundaries, while the bottom wall was set to either convection to air or adiabatic conditions in order to assess the importance of different heat loss mechanisms. The upper heater surface was set to a temperature-dependent convection condition by means of a user-defined function (UDF). The UDF approximated convective boiling with the working fluid FC-72 at its saturation temperature 329 K. Heat transfer coefficients were temperature-dependent, with values based on the FC-77 pool boiling experiment of Jones et al. [15]. Heat transfer coefficients above the glass surface were also temperature-dependent, with values based on the single-phase portion of the FC-77 curves of [15]. Heat input to the test strip was modeled as a volumetric heat generation in the very thin ITO heater half-domain.

Results of the parametric study shown in Fig. 7b indicate that measured values of heat flux would be subject to large errors, particularly for the narrower heater strips, if not corrected using the numerical model. It is apparent from the plot that, as the representative length scale (the heater half-width) decreases, even a thermal insulator such as borosilicate glass ($k_s \approx 1.4$ W/m K) can lead to effective extended surface heat transfer.

The 400-μm test strip was selected for boiling tests due to its lower spreading heat loss than the 100-μm test strip and clearer visualizations than the 1600-μm test strip. The boundary conditions in the numerical model were then modified to simulate each individual test condition as closely as possible, with heat generation within the 400-μm test strip set to the experimental value. The fundamental assumption of the numerical model is that the relationship between heat transfer coefficient and temperature expressed by the average boiling curve for the entire surface is also true for the spatially varying temperature field associated with a particular test condition. Therefore, an estimate of the true boiling curve for a surface is needed for the convection boundary condition UDF. The single phase regime was modeled as:

$$q = C(\Delta T)^{1.25}, \tag{3}$$

or $$h = C(\Delta T)^{0.25} \tag{4}$$

where the coefficient C is a parameter to be optimized and the ΔT dependence follows the natural convection formulation for the upward-facing surfaces of horizontal plates at lower Rayleigh numbers [43]. An upper limit of temperature was specified for the natural convection portion of each boiling curve by inspection of the data. Heat transfer coefficients for the boiling portion of the curve were piecewise linear between best estimate values corresponding to the experimental data points. The FLUENT model was then run as a feedback loop in which a new, improved estimate of the boiling curve was obtained after each converged set of results:

$$C_{new} = C_{old}\left[1 - \omega \cdot \frac{\sum_i (T_{w,\exp,i} - T_{w,calc,i})}{\sum_i \Delta T_{w,\exp,i}}\right], \tag{5}$$

$$\text{and } q_{new} = q_{old}\left[1 - \omega \cdot \frac{\Delta T_{w,\exp} - \Delta T_{w,calc}}{\Delta T_{w,\exp}}\right] \tag{6}$$

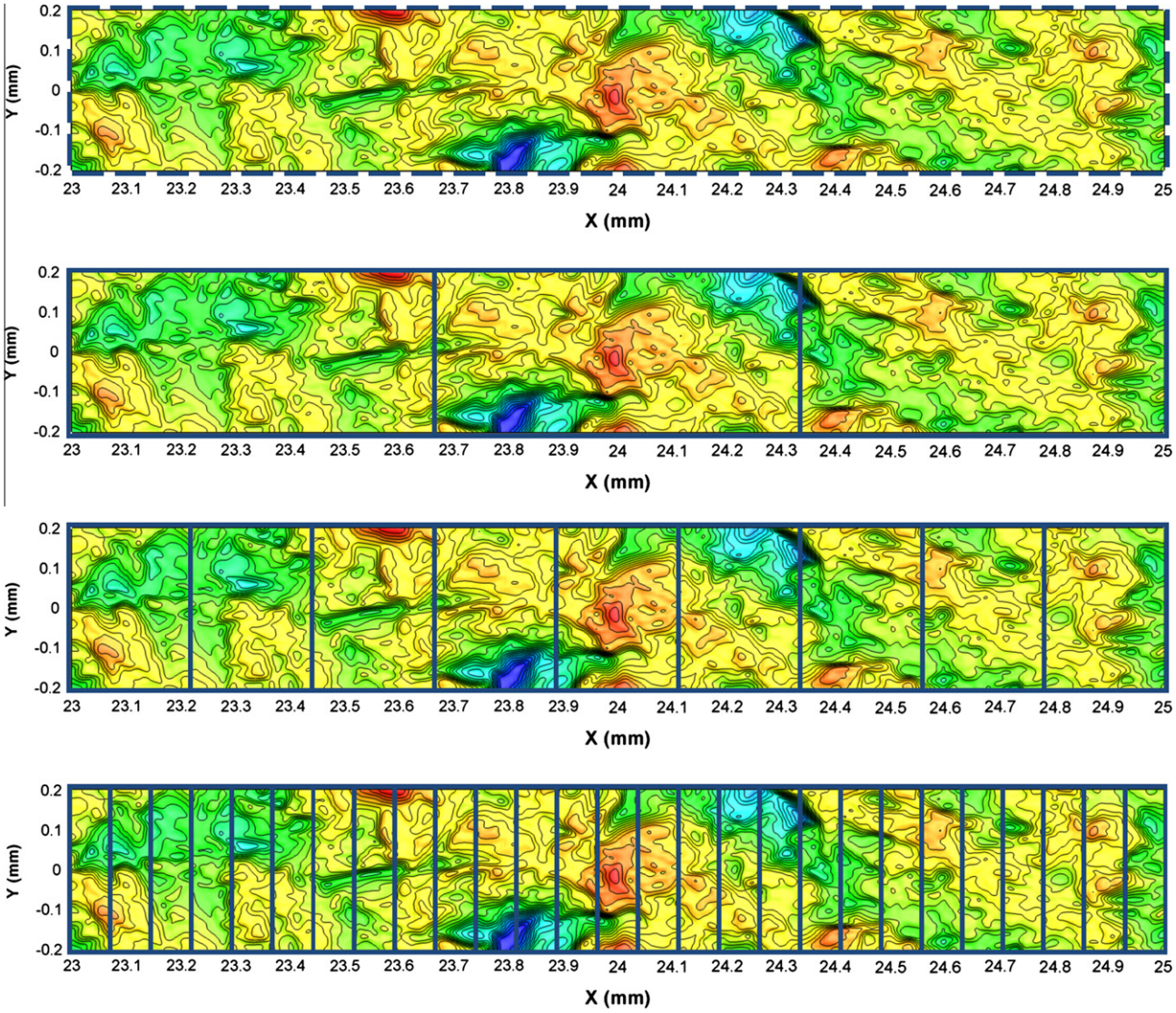

Fig. 8. Interrogation windows were selected over multiple length scales for calculation of average R_a and R_q surface roughness parameters (only the portion of the surface between $x = 23$ mm and $x = 25$ mm is shown for clarity of illustration).

$$\text{or } h_{new} = h_{old}\left[\Delta T_{w,calc} - \omega \cdot \frac{\Delta T_{w,\exp} - \Delta T_{w,calc}}{\Delta T_{w,\exp} \cdot \Delta T_{w,calc}}\right]. \quad (7)$$

The default value of the feedback underrelaxation factor ω was unity, although in some cases it needed to be reduced initially in order to prevent negative values for h.

Upon convergence of the FLUENT model for each feedback loop iteration, the mean surface temperature of the simulated test strip was calculated. New guesses obtained from Eqs. (6) and (7) were fed into the feedback loop, calling the FLUENT model repeatedly until the apparent boiling curves from the experiment were reproduced with minimal error. Root-mean-square (RMS) errors in temperature between reproduced and experimental boiling curves were about 0.5 K on average and are given in Table 3. Sensitivity of the heat flux values to changes in input temperature suggest that the uncertainty in individual heat flux values calculated from the numerical simulations is around 20% for the nucleate boiling portion of the curve.

5.2. Characterization of heater surface roughness

Comprehensive measurement of the surface roughness features is described here. Complete 3D maps of each test strip measuring 25 mm × 400 μm were obtained with a Zygo Newview 6200 white-light optical interferometer at 50× magnification. A white-light interferometer can only resolve very steep asperity angles at such a high magnification; the amount of x–y–z data for entire test strips at this magnification, however, exceeded the software stitching limitations of the instrument. The profile data for individual scans were therefore stitched together using a custom MATLAB [44] code. Alignment features on the part were used to map the part coordinate system (with origin at the center of the edge between the left electrode and the 400-μm test strip, and the test strip extending in the positive x-direction) to the instrument coordinate system. The resulting irregular data points were Delaunay-triangulated using the MATLAB command *TriScatteredInterp()* and mapped onto the regular mesh grid with x-range [0,25] and y-range [−0.2, 0.2] and identical x- and y-dimension spatial resolution using the function's linear interpolation option. Missing data points (*NaN* values) were automatically filled by the triangulation-interpolation scheme.

R_a and R_q values shown in Table 1 were calculated for the entire surface. There is no clear standard for the length scale that these measurements should span. Therefore, R_a and R_q were calculated for interrogation windows of 400 μm length (y) and widths (x) ranging from 1.767 μm (the horizontal resolution of the instru-

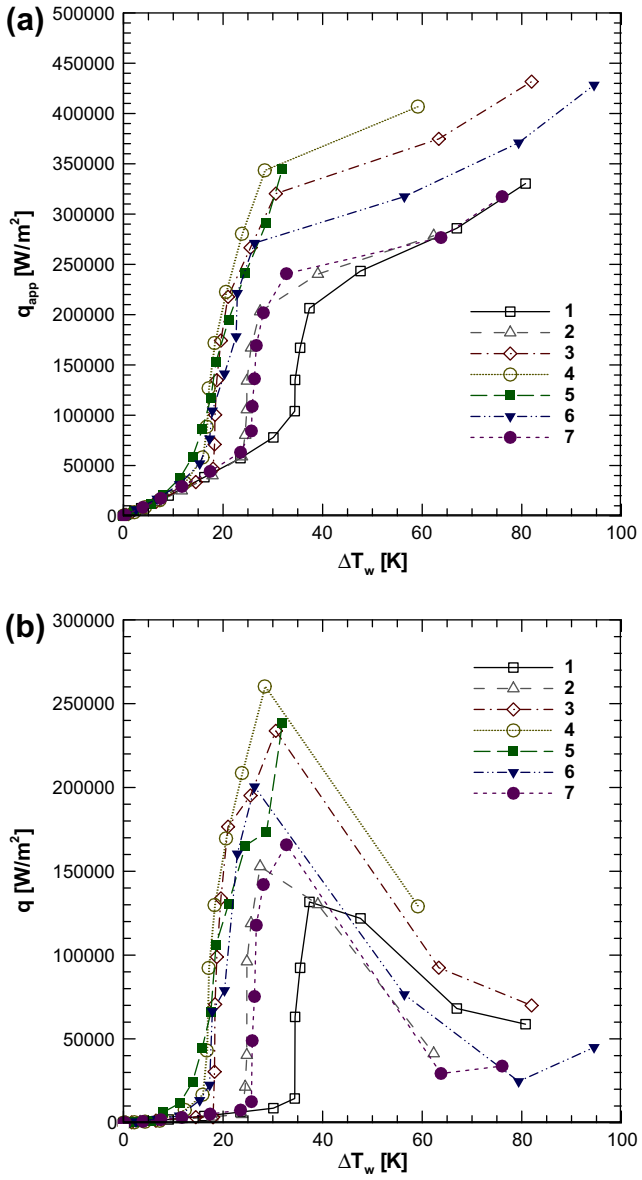

Fig. 9. Boiling curves for the seven surfaces tested: (a) apparent (uncorrected) heat flux values, and (b) heat flux values corrected by the method of Section 5.1.

ment) to 25 mm. For each window, a base plane was fit to the data and the deviations from this plane were used in the calculations. For interrogation widths less than 25 mm, all possible non-overlapping interrogation windows (as shown in Fig. 8) were evaluated and the values averaged. The lowest values invariably resulted from the smallest interrogation windows and highest values typically from the largest interrogation windows. The lowest R_a values are used in all plots and calculations in this paper and the companion paper [25] for the sake of consistency; it is noted that the low and high values calculated for each surface were not very different from each other (as shown in Table 1).

6. Results

Pool boiling experiments were carried out for the 400-μm test strips on all seven surfaces. Apparent (uncorrected) boiling curves for the seven surfaces are shown in Fig. 9a, and the corrected heat flux values accounting for spreading in the substrate by the method of Section 5.1 are shown in Fig. 9b. In this section, properties of the boiling curves are used to assess the quality of data obtained from the novel devices described in the present work. Quantitative and qualitative evaluations of the effect of surface roughness on boiling heat transfer and bubble nucleation characteristics are provided. Full statistical analyses of the heat transfer and bubble measurement data are presented in the companion paper [25].

6.1. Support for reported measurements

To the authors' knowledge, ITO devices have not successfully been used as temperature sensors in any other study of boiling heat transfer, and few pool boiling experiments rely so heavily upon numerical simulation to determine heat flux values. Additional evidence that the measurements reported here are accurate is provided by the following internal consistencies.

All uncorrected boiling curves contain a nearly identical natural convection portion, which further validates the approach used to calibrate and measure temperature with the ITO devices. Natural convection heat transfer is the result of transient conduction into the fluid, subject to the instability-related time scale [45]. As such, micron-scale roughness can have little effect on the heat transfer since the surfaces are well wetted, i.e., there is good thermal contact between solid and liquid for all surfaces. Heat flux vs temperature curves for different surfaces in the single-phase regime would therefore be expected to be identical, which is the present case despite that each devices has been independently calibrated.

After applying the heat flux correction, the natural convection portions of the various curves are still nearly identical. The numerical heat loss simulation applies the natural convection portion of the curve over much of the upper surface of the test piece when optimizing the estimate of the true boiling curve in the feedback loop. Thus the calculated heat flux values for the boiling portion of the curve are thermally coupled to the natural convection portion. Since simulated values of natural convection are consistent and the same for different surfaces, the boiling portions of the curves must also be consistent (though different). The calculated boiling curves can therefore be compared with a good degree of accuracy, even if an individual heat flux data point may only be certain to within about 20%.

6.2. Effect of surface roughness on boiling heat transfer

Boiling curves for the roughened surfaces are characterized by ΔT_w values significantly less than those for the smoother surfaces, as expected. The R_a values of surfaces 1–7 cover a wide range, while the boiling curves seem to lie along only three paths. Surprisingly, the boiling curves for surfaces 2 and 7 are almost identical, while the R_a value of surface 7 suggests that it should have similar performance to surface 3 instead of surface 2. From Table 1, it can be seen that the annealing conditions of surface 7 are more aggressive than for the other surfaces. Fig. 1 shows that these annealing conditions cause the fine-scale roughness features to disappear. Clearly, R_a does not consistently indicate the heat transfer performance of a surface; the R_a measurement ignores fine scale roughness if larger scale asperities are present.

Surface roughness is clearly a parameter of importance in determining critical heat flux as well as wall superheat. All surfaces reached critical heat flux except for surface 5, which did not reach an identifiable point of critical heat flux despite the appearance of dry patches on the surface at the highest value of apparent heat flux, 345,000 W/m^2 as shown in Fig. 9a. Approximate values of critical heat flux (CHF) may be inferred from the data for the other surfaces. The wall superheat at the apparent point of CHF for surfaces 2–7 averaged 29.7 K except for the polished surface, for which $\Delta T_{w,CHF}$ was 38.5 K. The corrected critical heat flux q_{CHF} varied

Table 4
Visual comparison of nucleate boiling from smooth and rough surfaces. The upper image in each block is the side view, while the lower image is the bottom view. Scale markings shown in bottom view images are 500 μm long and spaced 500 μm apart.

Experimental Conditions	Surface 1	Surface 6	Experimental Conditions
q = 8,700 W/m^2 ΔT_w = 30.1 K	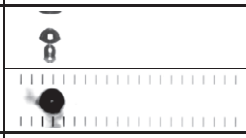	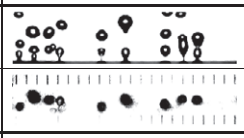	q = 13,300 W/m^2 ΔT_w = 15.3 K
q = 14,500 W/m^2 ΔT_w = 34.4 K	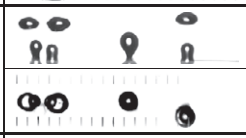	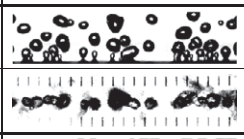	q = 22,500 W/m^2 ΔT_w = 17.3 K
q = 63,130 W/m^2 ΔT_w = 34.5 K	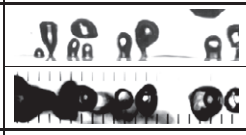	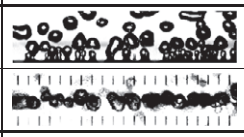	q = 66,400 W/m^2 ΔT_w = 17.9 K
q = 92,400 W/m^2 ΔT_w = 35.5 K	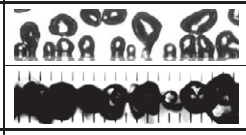	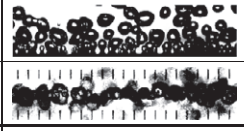	q = 78,900 W/m^2 ΔT_w = 20.3 K
q = 132,000 W/m^2 ΔT_w = 37.4 K	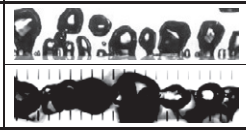	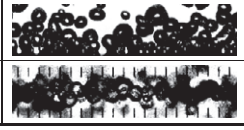	q = 117,000 W/m^2 ΔT_w = 22.6 K

between 147,000 W/m^2 for the polished surface and 265,000 W/m^2 for surface 4; q_{CHF} did not appear to correlate well with R_a.

Another interesting feature of the test surfaces may be seen by comparing Fig. 9a and b. Although normally absent for power-controlled surfaces, a 'transition' portion of the boiling curve beyond CHF is present and controllable. This is due to the fact that the test strip temperature is strongly coupled to the saturation temperature of the fluid by short conduction paths through the substrate.

6.3. Effects of surface roughness on bubble ebullition

High speed video was simultaneously recorded in bottom and side view orientations for each test condition in which boiling occurred, as summarized in Table 4. These results are quantitatively analyzed in the companion paper [25], but general features of the boiling are apparent by inspection. In the table, boiling images from surfaces 1 and 6, representative of smooth and rough surfaces, respectively, are compared for similar heat fluxes. Nucleation site densities are considerably higher for the rough surface. Average bubble departure diameters appear to be somewhat higher for the smooth surface. Departure frequencies, which can be observed in the accompanying videos, are not much different for smooth and rough surfaces. Boiling at values of q near CHF is characterized by large intermittent dry vapor patches at the base of macrobubbles (those formed by multiple mergers) remaining attached to the surface for somewhat prolonged periods. Macrobubbles are significantly larger and experience greater residence times on the smooth surface than individual bubbles.

The active site density may be limited for surface 1 by the number of potential nucleation sites, which contributes to its higher wall superheat for a given heat flux. Surface 6, being very rough, has an abundance of potential nucleation sites and many more sites active than surface 1. With more bubbles being generated per unit area, more of the area of surface 6 benefits from the four mechanisms of heat transfer [46] associated with bubble ebullition, rather than only the single-phase conduction mechanism. In addition, the bubbles generated by surface 6 seem to remain distinct from one another even at high heat fluxes; vapor patches do not spread beyond the base of a single bubble until a much higher surface heat flux than for surface 1. This may be explained by the higher wettability (lower fluid contact angle) on the rough surface, and it could explain [47] its higher CHF than the smooth surface 1.

7. Conclusions

A new type of pool boiling facility employing a transparent borosilicate glass substrate coated with indium tin oxide was developed. The primary strengths of this facility are: (1) the good degree of controllability of the surface roughness features, and (2) good optical access for high-quality visualizations from both the side and below the boiling surface. Variation of the ITO heater/sensor resistance with factors other than temperature was taken into account to an excellent degree by normalization with its resistance at the saturation temperature, which could be easily measured between boiling data points. Thermal spreading through the glass substrate was accounted for by 2-D numerical simulations. Surface roughness and liquid contact angle values were measured precisely for the heater surfaces. Resulting boiling curves revealed the importance of the structure as well as the size of surface roughness features. Visualizations of bubble ebullition revealed bubbles to be smaller and more distinct for a rough surface than for a smooth surface. Active nucleation site densities were higher for the rough surface, and the vapor in contact with the rough surface did not spread as freely as on the smooth surface.

Acknowledgments

Financial support for this work was provided by the Indiana 21st Century Research and Technology Fund and the Cooling Tech-

nologies Research Center at Purdue University. Ms. Suchismita Sarangi assisted in construction and operation of the experimental facility, and Mr. Steve Titolo offered useful insights about the facility design. The authors also thank Northrop Grumman Corporation for donating FC-72 working fluid and OPCO Laboratory of Fitchburg, MA for providing preliminary coating samples.

References

[1] M. Jakob, Heat transfer in evaporation and condensation-I, Mechanical Engineering 58 (1936) 643–660.
[2] W.M. Rohsenow, A method of correlating heat transfer data for surface boiling of liquids, Transactions of the ASME 74 (1952) 969–976.
[3] S.G. Bankoff, A.J. Hajjar, J.B.B. McGlothin, On nature and location of bubble nuclei in boiling from surfaces, Journal of Applied Physics 29 (1958) 1739–1741.
[4] S.G. Bankoff, Entrapment of gas in the spreading of a liquid over a rough surface, American Institute of Chemical Engineers Journal 4 (1958) 24–26.
[5] P. Griffith, J.D. Wallis, The role of surface conditions in nucleate boiling, Chemical Engineering Progress Symposium Series 56 (1960) 49–63.
[6] Y.Y. Hsu, On the size range of active nucleation cavities in a heating surface, Journal of Heat Transfer 84 (1962) 207–216.
[7] C. Corty, A.S. Foust, Surface variables in nucleate boiling, Chemical Engineering Progress Symposium Series 51 (1955) 1–12.
[8] P. Berenson, Experiments on pool boiling heat transfer, International Journal of Heat and Mass Transfer 5 (1962) 985–999.
[9] R. Vachon, G. Nix, G. Tanger, Evaluation of constants for the Rohsenow pool-boiling correlation, Journal of Heat Transfer 90 (1968) 239–247.
[10] I.L. Pioro, Experimental evaluation of constants for the Rohsenow pool boiling correlation, International Journal of Heat and Mass Transfer 42 (1998) 2003–2013.
[11] H.M. Kurihara, J.E. Myers, The effects of superheat and surface roughness on boiling coefficients, American Institute of Chemical Engineers Journal 6 (1960) 83–91.
[12] K. Bier, D. Gorenflo, M. Salem, Y. Tanes, Pool boiling heat transfer and size of active nucleation centers for horizontal plates with different surface roughness, in: Sixth International Heat Transfer Conference, Hemisphere Publishing Corp, Washington, DC, USA, 1978, pp. 151–156.
[13] M.G. Kang, Effect of surface roughness on pool boiling heat transfer, International Journal of Heat and Mass Transfer 43 (2000) 4073–4085.
[14] A. Luke, Pool boiling heat transfer from horizontal tubes with different surface roughness, International Journal of Refrigeration 20 (1997) 561–574.
[15] B.J. Jones, J.P. McHale, S.V. Garimella, The influence of surface roughness on nucleate pool boiling heat transfer, Journal of Heat Transfer 131 (2009) 121009.
[16] R. Benjamin, A. Balakrishnan, Nucleation site density in pool boiling of saturated pure liquids: effect of surface microroughness and surface and liquid physical properties, Experimental Thermal and Fluid Science 15 (1997) 32–42.
[17] A. Luke, Preparation and analysis of different roughness structures for evaporator tubes, Heat and Mass Transfer 45 (2009) 909–917.
[18] B.J. Jones, Fundamental Studies of Thermal Transport and Liquid–Vapor Phase Change Using Microscale Diagnostic Techniques, PhD Thesis, Purdue University, West Lafayette, IN, 2010.
[19] M. Cooper, Saturation nucleate pool boiling: a simple correlation, in: 1st UK National Conference on Heat Transfer, 1984, pp. 785–793.
[20] T. Hibiki, M. Ishii, Active nucleation site density in boiling systems, International Journal of Heat and Mass Transfer 46 (2003) 2587–2601.
[21] C. Yang, Y. Wu, X. Yuan, C. Ma, Study on bubble dynamics for pool nucleate boiling, International Journal of Heat and Mass Transfer 43 (2000) 203–208.
[22] H.C. Lee, B.D. Oh, S.W. Bae, M.H. Kim, Single bubble growth in saturated pool boiling on a constant wall temperature surface, International Journal of Multiphase Flow 29 (2003) 1857–1874.
[23] V.P. Carey, Liquid–Vapor Phase-Change Phenomena: An Introduction to the Thermophysics of Vaporization and Condensation, Hemisphere Publishing Corp., Washington, DC, 1992.
[24] J.P. McHale, S.V. Garimella, Bubble nucleation characteristics in pool boiling of a wetting liquid on smooth and rough surfaces, International Journal of Multiphase Flow 36 (2010) 249–260.
[25] J.P. McHale, S.V. Garimella, Nucleate boiling from smooth and rough surfaces – Part 2: analysis of surface roughness effects on nucleate boiling, Experimental Thermal Fluid Science, http://dx.doi.org/10.1016/j.expthermflusci.2012.08.005.
[26] H. Wensink, S. Schlautmann, M.H. Goedbloed, M.C. Elwenspoek, Fine tuning the roughness of powder blasted surfaces, Journal of Micromechanics and Microengineering 12 (2002) 616–620.
[27] AZ Electronic Materials, AZ 9260 Data Package, <http://www.nanofab.utah.edu/svn/public/documents/Non%20SOPs/Photoresist/az_9260_photoresist.pdf>, 2007 (accessed 06.10).
[28] 3M Corporation, Fluorinert Electronic Liquid FC-72 Product Information, St. Paul, MN, 2000.
[29] 3M Corporation, Fluorinert Liquids Product Manual, St. Paul, MN, 1986.
[30] C.C. Pascual, S.M. Jeter, S.I. Abdel-Khalik, Visualization of boiling bubble dynamics using a flat uniformly heated transparent surface, International Journal of Heat and Mass Transfer 45 (2002) 691–696.
[31] O.J. Gregory, T. You, Ceramic temperature sensors for harsh environments, Sensors Journal IEEE 5 (2005) 833–838.
[32] M. Mizuhashi, Electrical properties of vacuum-deposited indium oxide and indium tin oxide films, Thin Solid Films 70 (1980) 91–100.
[33] W. Fritz, Berechnung des maximalvolume von dampfblasen, Physikalische Zeitschrift 36 (1935) 379–388.
[34] J.J. Lorenz, B.B. Mikic, W.M. Rohsenow, Effect of surface conditions on boiling characteristics, in: Proc. 5th International Heat Transfer Conference, Hemisphere, Tokyo, 1974, pp. 35–39.
[35] W. Tong, A. Bar-Cohen, T.W. Simon, S.M. You, Contact angle effects on boiling incipience of highly-wetting liquids, International Journal of Heat and Mass Transfer 33 (1990) 91–103.
[36] Y. Qi, J.F. Klausner, Heterogeneous nucleation with artificial cavities, Journal of Heat Transfer 127 (2005) 1189–1196.
[37] K. Cornwell, On boiling incipience due to contact angle hysteresis, International Journal of Heat and Mass Transfer 25 (1982) 205–211.
[38] A.M. Schwartz, S.B. Tejada, Studies of dynamic contact angles on solids, Journal of Colloid and Interface Science 38 (1972) 359–375.
[39] A. Mukherjee, S.G. Kandlikar, Numerical study of single bubbles with dynamic contact angle during nucleate pool boiling, International Journal of Heat and Mass Transfer 50 (2007) 127–138.
[40] H.Y. Erbil, G. McHale, M.I. Newton, Drop evaporation on solid surfaces: constant contact angle mode, Langmuir 18 (2002) 2636–2641.
[41] C. Bourges-Monnier, M.E.R. Shanahan, Influence of evaporation on contact angle, Langmuir 11 (1995) 2820–2829.
[42] Fluent Inc., FLUENT 6.2 User's Guide, Lebanon, NH, 2005.
[43] F. Incropera, D. DeWitt, Free Convection, in: Fundamentals of Heat and Mass Transfer, John Wiley & Sons, New York, 2002. pp. 539–592.
[44] The Mathworks Inc., MATLAB Version 7.8.0, Natick, Massachussetts, 2009.
[45] A. Bejan, Convection Heat Transfer, John Wiley & Sons, Hoboken, New Jersey, 2004 (Chapters 4–5).
[46] S. Moghaddam, K. Kiger, Physical mechanisms of heat transfer during single bubble nucleate boiling of FC-72 under saturation conditions. II: Theoretical analysis, International Journal of Heat and Mass Transfer, 52 (2009) 1295–1303.
[47] T.G. Theofanous, J.P. Tu, A.T. Dinh, T.N. Dinh, The boiling crisis phenomenon: Part I: Nucleation and nucleate boiling heat transfer, Experimental Thermal and Fluid Science 26 (2002) 775–792.